

Constraints on the cosmological parameters with three-parameter correlation of Gamma-ray bursts

JIA-LUN LI,¹ YU-PENG YANG,¹ SHUANG-XI YI[†],¹ JIAN-PING HU,² FA-YIN WANG,² AND YAN-KUN QU¹

¹*School of Physics and Physical Engineering, Qufu Normal University, Qufu 273165, China; yisx2015@qfnu.edu.cn, ypyang@qfnu.edu.cn*

²*School of Astronomy and Space Science, Nanjing University, Nanjing 210023, China; fayinwang@nju.edu.cn*

ABSTRACT

As one of the most energetic and brightest events, gamma-ray bursts (GRBs) can be treated as a promising probe of the high-redshift universe. Similar to type Ia supernovae (SNe Ia), GRBs with same physical origin could be treated as standard candles. We select GRB samples with the same physical origin, which are divided into two groups. One group is consisted of 31 GRBs with a plateau phase feature of a constant luminosity followed by a decay index of about -2 in the X-ray afterglow light curves, and the other has 50 GRBs with a shallow decay phase in the optical light curves. For the selected GRB samples, we confirm that there is a tight correlation between the plateau luminosity L_0 , the end time of plateau t_b and the isotropic energy release $E_{\gamma,iso}$. We also find that the $L_0 - t_b - E_{\gamma,iso}$ correlation is insensitive to the cosmological parameters and no valid limitations on the cosmological parameters can be obtained using this correlation. We explore a new three-parameter correlation L_0 , t_b , and the spectral peak energy in the rest frame $E_{p,i}$ ($L_0 - t_b - E_{p,i}$), and find that this correlation can be used as a standard candle to constrain the cosmological parameters. By employing the optical sample only, we find the constraints of $\Omega_m = 0.697_{-0.278}^{+0.402}(1\sigma)$ for a flat Λ CDM model. For the non-flat Λ CDM model, the best-fitting results are $\Omega_m = 0.713_{-0.278}^{+0.346}$, $\Omega_\Lambda = 0.981_{-0.580}^{+0.379}(1\sigma)$. For the combination of the X-ray and optical samples, we find $\Omega_m = 0.313_{-0.125}^{+0.179}(1\sigma)$ for a flat Λ CDM model, and $\Omega_m = 0.344_{-0.112}^{+0.176}$, $\Omega_\Lambda = 0.770_{-0.416}^{+0.366}(1\sigma)$ for a non-flat Λ CDM model.

Keywords: cosmological parameters; magnetar; Gamma-ray burst

1. INTRODUCTION

Gamma-ray bursts (GRBs) are among the most energetic explosive events with a luminosity $L \sim 10^{47} - 10^{54}$ erg s⁻¹ in the Universe (Klebesadel et al. 1973; Mészáros 2006; Gehrels et al. 2009; Wang & Dai 2011; Kumar & Zhang 2015). Based on the distribution of the bimodal duration time T_{90} , GRBs are typically divided into two categories of short GRBs (SGRBs, $T_{90} < 2s$) and long GRBs (LGRBs, $T_{90} > 2s$) (Kouveliotou et al. 1993; Qin et al. 2013). The LGRBs most likely originate from the collapses of the massive stars (Woosley 1993; Paczyński 1998; MacFadyen & Woosley 1999; MacFadyen et al. 2001). The progenitors of SGRBs stem from the merger of two neutron stars (NS) or a NS and a black hole (BH) in the system of binary (Woosley & Bloom 2006; Gehrels et al. 2009; Abbott et al. 2017; Tang et al. 2021). At present, the maximum redshift of GRB observed is $z \sim 9.4$ (Cucchiara et al. 2011), and they could be detected up to $z \sim 20$ (Lamb & Reichart 2000). Therefore, GRBs can be used to investigate the characters of the Universe at high-redshift (Dai et al. 2004; Ghirlanda et al. 2004a; Liang & Zhang 2006; Schaefer 2007; Ko-

dama et al. 2008; Wang et al. 2011; Amati & Della Valle 2013; Wei & Wu 2017; Wei et al. 2018; Khadka et al. 2021; Dainotti et al. 2022a,b). On the other hand, SNe Ia (Phillips 1993; Riess et al. 1998; Perlmutter et al. 1999) and the cosmic microwave background (CMB) (Spergel et al. 2003; Planck Collaboration et al. 2014, 2016, 2020) have been successfully used as cosmological probes. Due to the physical mechanism of SNe Ia, its maximum luminosity is limited, leading to the detected upper limit of redshift is not very large. The CMB provides relevant information about the early universe. From this point of view, GRBs are regarded as a complement to SNe Ia and CMB. Moreover, gamma-ray photons are largely unaffected by the interstellar medium (ISM) that SNe Ia faces as they travel towards us (Wang et al. 2015).

Similar to SNe Ia, GRBs can be standardized to be a cosmic distance indicator for cosmological purposes by using correlations between their observable quantities (Cao et al. 2022a,b,c; Jia et al. 2022; Liang et al. 2022; Liu et al. 2022; Li et al. 2023a). In general, the relations can be divided into three main categories: (1) the correlations observed in the prompt phase of the emission

including the Amati correlation (Amati et al. 2002), the Ghirlanda correlation (Ghirlanda et al. 2004b), and the Yonetoku correlation (Yonetoku et al. 2004); (2) the afterglow correlations involving the Dainotti correlation of $L_0 - t_b$ (Dainotti et al. 2008), (3) the prompt-afterglow correlations including Liang-Zhang correlation (Liang & Zhang 2005). There have been extensive investigations on the Dainotti relation, which is a correlation between the plateau luminosity L_0 and the end time of the plateau t_b . Moreover, there are many studies that have used the Dainotti relation to measure cosmological parameters (Cardone et al. 2009, 2010; Dainotti et al. 2013; Postnikov et al. 2014; Izzo et al. 2015; Levine et al. 2022). Wang et al. (2016) have used the Dainotti relation to standardize the afterglow light curves of long GRBs, and the GRB samples are divided into gold and silver sample groups according to the behaviors of the light curves. Hu et al. (2021) conducted updated investigations with SGRBs whose spin-down is dominated by magnetic dipole (MD) radiations (MD-SGRBs) and LGRBs whose spin-down is dominated by gravitational wave (GW) emission (GW-LGRBs). The method has been proposed by Xu & Huang (2012) to extend the Dainotti relation by adding the isotropic energy $E_{\gamma,iso}$ into the $L_0 - t_b$ relation and found a much tighter correlation than that of two-parameter. Here we will use the relation $L_0 - t_b - E_{\gamma,iso}$ to probe the cosmological parameters. Moreover, since the correlation between $E_{\gamma,iso}$ and the spectral peak energy in the rest frame $E_{p,i}$ (Amati et al. 2002), we will also investigate whether $L_0 - t_b - E_{p,i}$ correlation can be used to probe the cosmological parameters. Xu et al. (2021) have used the relations $L_0 - t_b - E_{\gamma,iso}$ and $L_0 - t_b - E_{p,i}$ to constrain the cosmological parameters, based on a sample including 121 long GRBs. We will study these two correlations by employing different samples.

If the central engine of a GRB is powered by a newly born fast spinning neutron star with high magnetic field, the energy injection from the magnetar could cause the plateau phase in the X-ray light curves (Dai & Lu 1998b; Zhang & Mészáros 2001; Metzger et al. 2011). Based on the observations of Swift (Gehrels et al. 2004), a significant fraction of GRBs shows a plateau phase in the X-ray light curves followed by a decay phase in afterglows (Zhang et al. 2006; Nousek et al. 2006; O’Brien et al. 2006; Liang et al. 2007; Yi et al. 2015, 2016; Li et al. 2023b). This characteristic of the light curve could be explained by the possibility that the energy injection from the magnetar causes a shallow decline phase in afterglows (Dai & Lu 1998b; Zhang & Mészáros 2001). Dai & Lu (1998b) have suggested that the rotational energy of a newly born magnetar is released as the gravitational

wave and electromagnetic radiation, leading to the neutron star spin down. If the spin down is dominated by magnetic dipole radiation (MD-radiation), the corresponding luminosity evolving with time can be written as (Dai & Lu 1998b)

$$L = L_0 \times \frac{1}{(1 + t/t_b)^2} \simeq \begin{cases} L_0 & t \ll t_b, \\ L_0(t/t_b)^{-2} & t \gg t_b, \end{cases} \quad (1)$$

where L_0 and t_b represent the characteristic spin-down luminosity and end time of the plateau, respectively. The values of these parameters can be obtained by fitting the X-ray afterglow light curves with the plateau phase.

In recent years, SNe Ia have been studied extensively as a well-established class of standard candle, since SNe Ia with the same source of systematics have a nearly uniform luminosity with an absolute magnitude $M \simeq -19.5$ (Carroll 2001). Similar to SNe Ia, GRBs with plateau phase caused by the same physical mechanism should be standardized as standard candles.

Recently, GRBs have been classified in more detail with different decay indices (Wang et al. 2022). These classified GRBs are then standardized using Dainotti correlation, and a more tight cosmological constraints are obtained. According to the observations of Swift, many long-GRBs have a trait of plateau phase and a normal decay phase. Additionally, an analogous shallow decay phase also appears in the optical afterglow of GRBs. These shallow decay phase of optical light curves should have a similar physical mechanism. Therefore, similar to the case of X-ray, the classification of optical light curves is also based on the decay indices.

Si et al. (2018) have found that the correlations of $L_0 - t_b - E_{\gamma,iso}$ or $L_0 - t_b - E_{p,i}$ are tighter than that of $L_0 - t_b$. In this work, we will investigate the selected X-ray and optical samples, whose spin-down is potentially dominated by the same physical mechanism, and standardize them using the correlation of $L_0 - t_b - E_{\gamma,iso}$ and $L_0 - t_b - E_{p,i}$. In the next section, we will briefly introduce the sample selection. In Sec. III, we standardize X-ray and optical samples utilizing the correlations of $L_0 - t_b - E_{\gamma,iso}$ and $L_0 - t_b - E_{p,i}$. In Sec. IV, we use the standardized samples to constrain the cosmological parameters for Λ CDM model, and discuss which correlation is better for probing the Universe at higher redshifts. The conclusions are given in Sec. V.

2. SAMPLE SELECTION OF GRBS

As previously stated, if the central engine of a GRB is powered by a newly born magnetar, the continuous energy injection from magnetar will cause a plateau phase

in the X-ray light curves (Dai & Lu 1998b; Zhang & Mészáros 2001; Metzger et al. 2011). The energy reservoir of newly born magnetized neutron star is rotational energy, and the spin-down of a newly born magnetar is through a combination of the electromagnetic dipole radiation and gravitational wave emission. If the spin-down of newly born magnetar is dominated by MD-radiation, the light curves of X-ray afterglow will show a plateau followed by a normal decay phase with a decay index of about -2. On the other hand, if the spin-down is dominated by GW-emission, the decay index is about -1 for the X-ray afterglow light curves.

These predictions have been confirmed by the Swift observations, and part of GRBs are characterized by a plateau phase followed by a normal decay phase in the early X-ray afterglow. Tang et al. (2019) conducted a statistical investigation of 174 GRBs with a plateau phase in the X-ray afterglow. It has been discovered that a tight correlation between L_0 and t_b (Dainotti relation) (Dainotti et al. 2008) can be used to measure the cosmological parameters by investigating the GRBs with X-ray afterglow plateau phases (Cardone et al. 2009, 2010; Dainotti et al. 2013; Postnikov et al. 2014; Izzo et al. 2015). Whereas, the results of the cosmological constraints are loose, and the main reason is the samples are not well selected (Wang et al. 2022). Similar to the supernova cosmology, where only type Ia supernova caused by the same physical mechanism can serve as standard candles, GRBs with an X-ray plateau potentially generated by the same physical mechanism are selected. The decaying indices of the X-ray light curves could be explained by the loss of rotational energy of magnetar in different ways. Therefore, it is necessary to conduct a more detailed classification of GRBs according to different decay indices.

Wang et al. (2022) and Hu et al. (2021) have carefully selected and classified the GRB samples into several sample spaces, MD-SGRBs, MD-LGRBs, and GW-LGRBs according to the decay indices in the X-ray afterglow. These X-ray light curves are then standardized using Dainotti relation. Here we adopt 31 LGRBs selected by Wang et al. (2022), which are divided into gold and silver samples. The X-ray sample is selected using the following criteria.

- There are no weak flares, especially during the plateau.
- There are enough data points at plateau and decay phase, and the data points have good coverage of the light curve.
- There is an obvious plateau in gold sample, and an expected platform phase in silver sample by analyzing the XRT and BAT data.

- The duration time of decay phase is larger than $5t_b$.
- The plateau phase is followed by a decay index of about -2.

The selected samples can improve the reliability of the fitting, and are consistent with the fact that the energy injection of magnetar electromagnetic dipole emission is greater than the external shock emission (the decay index is about -1.2). Moreover, the X-ray afterglow light curves of all samples show a plateau stage with a constant luminosity followed by a decay stage with a decay index of about -2.

Not only do many GRBs exhibit a plateau phase in X-ray afterglow followed by a normal decay phase, but a similar decay phase also appear in the optical light curves. However, only a small part of the optical afterglow possesses a plateau phase (Li et al. 2012). This particular phase of shallow decay in the optical light curves may originate from the same physical process (Dai & Lu 1998a,b; Zhang & Mészáros 2001; Fan & Xu 2006; Liang et al. 2007; Rowlinson et al. 2013; Lü & Zhang 2014; Yi et al. 2022). Si et al. (2018) screened 50 GRBs samples from the published literature for the studies of the correlation of optical plateaus. The selection criteria for optical sample are similar to those for X-rays. The optical sample is selected in terms of the following criteria.

- There is an obvious plateau stage in the optical afterglow curve, where a shallow decay or a slight rising phase is allowed.
- The plateau phase is followed by a normal decay or an even steeper decay (such as GRB 030429).

The selected well-sampled afterglows with obvious plateau stage are the transition of the optical afterglow light curves from a shallow decay (or a slight rising phase) to normal decay (or an even steeper decay). It is worth noting that GRBs 050319, 060526 and 080310 are included in both groups of samples. We will use these selected 50 optical sample and 31 X-ray sample for our studies.

3. THE THREE-PARAMETER CORRELATION OF X-RAY AND OPTICAL SAMPLES

3.1. *Fitting the correlation*

With the plateau flux F_0 obtained, the luminosity L_0 of the plateau phase can be written as

$$L_0 = \frac{4\pi d_L^2 F_0}{(1+z)}, \quad (2)$$

where d_L is the luminosity distance. For the X-ray luminosity, K-correction of $(1+z)^{1-\beta}$ should be included, where β is the spectral index of the plateau phase. In

the flat universe model, the luminosity distance d_L can be written as

$$d_L = \frac{c(1+z)}{H_0} \int_0^z \frac{dz}{\sqrt{\Omega_m(1+z)^3 + \Omega_\Lambda}}, \quad (3)$$

where Ω_m and Ω_Λ represent the density parameters of matter and dark energy, respectively.

Wang et al. (2022) have pointed out that for a group of GRBs (e.g., the GRBs with redshift $z < 0.1$), if their distances can be obtained directly by observation, the deriving $L_0 - t_b$ correlation is model-independent. The relationship between two parameters L_0 and t_b can be written as follows

$$\log\left(\frac{L_0}{10^{47} \text{erg s}^{-1}}\right) = k \times \log\frac{t_b}{10^3(1+z)s} + b. \quad (4)$$

Wang et al. (2022) has fitted the $L_0 - t_b$ relation using X-ray sample. Furthermore, for a group of X-ray plateau samples, a much tighter three-parameter correlation of $L_0 - t_b - E_{\gamma,iso}$ is obtained with the isotropic energy release $E_{\gamma,iso}$ (Xu & Huang 2012; Deng et al. 2023). Si et al. (2018) studied the relationship of $L_0 - t_b - E_{\gamma,iso}$ by using the well-sampled optical light curves of 50 GRBs. Similar to the $L_0 - t_b$ relation, the $L_0 - t_b - E_{\gamma,iso}$ relation can be expressed as

$$\log\frac{L_0}{10^{47} \text{erg s}^{-1}} = a + b \log\frac{t_b}{10^3 s} + c \log\frac{E_{\gamma,iso}}{10^{53} \text{erg}}, \quad (5)$$

where a , b and c can be determined by fitting observed data¹. The isotropic energy of the prompt emission is

$$E'_{\gamma,iso} = \frac{4\pi d_L^2 S}{1+z}, \quad (6)$$

where S is the fluence. Due to cosmological time dilaton, the energy bands of the observer frame and rest frame are different. Therefore, K-correction should be considered in the calculation of $E_{\gamma,iso}$. Including K-correction $E_{\gamma,iso}$ can be written as

$$E_{\gamma,iso} = E'_{\gamma,iso} \times \frac{\int_{E_1/1+z}^{E_2/1+z} E\phi(E)dE}{\int_{E_1}^{E_2} E\phi(E)dE}, \quad (7)$$

where E_2 and E_1 are the upper and lower limits of the detector energy range, respectively. $\phi(E)$ is the energy spectrum, which can be modeled with a smoothly broken power law (Band et al. 1993),

$$\phi(E) = \begin{cases} AE^\alpha e^{-(2+\alpha)E/E_{p,obs}} & , E \leq \frac{\alpha-\beta}{2+\alpha} E_{p,obs}, \\ BE^\beta & , E > \frac{\alpha-\beta}{2+\alpha} E_{p,obs}, \end{cases} \quad (8)$$

where α and β are the power-law index of photon energies below and above the break, respectively. $E_{p,obs}$ is the observed peak energy.

The best fitting results of a , b , c , and the intrinsic scatter σ_{int} can be obtained by using the likelihood function. The corresponding likelihood can be written as (D'Agostini 2005)

$$\mathcal{L}(a, b, c, \sigma_{int}) \propto \prod_i \frac{1}{\sqrt{\sigma_{int}^2 + \sigma_{y_i}^2 + b^2 \sigma_{x_{1,i}}^2 + c^2 \sigma_{x_{2,i}}^2}} \times \exp\left[-\frac{y_i - a - bx_{1,i} - cx_{2,i}}{2(\sigma_{int}^2 + \sigma_{y_i}^2 + b^2 \sigma_{x_{1,i}}^2 + c^2 \sigma_{x_{2,i}}^2)}\right], \quad (9)$$

where σ_{int} is the extrinsic parameter. Here we have set $x_1 = \log(t_b/10^3 s)$, $x_2 = \log(E_{\gamma,iso}/10^{47} \text{erg})$ and $y = \log(L_0/10^{47} \text{erg s}^{-1})$ (for optical sample $y = \log(L_0/10^{44} \text{erg s}^{-1})$). The minimization is performed employing the Markov Chain Monte Carlo (MCMC) algorithm with the `emcee` package (Foreman-Mackey et al. 2013). Using X-ray afterglow sample with the platform stage, we find a tighter three-parameter correlation compared with the previous two-parameter correlation. Figure 1 shows the correlation of equation 5 for the X-ray and optical samples. The best fitting results for the X-ray sample shown on the left panel are $a = 2.033 \pm 0.144$, $b = -1.021 \pm 0.092$, $c = 0.538 \pm 0.144$ and $\sigma_{int} = 0.303 \pm 0.043$, corresponding to $L_0 \propto t_b^{-1.021 \pm 0.092} E_{\gamma,iso}^{0.538 \pm 0.144}$. The figure on the right shows that the best fitting results for optical sample are $a = 2.044 \pm 0.149$, $b = -0.944 \pm 0.098$, $c = 0.369 \pm 0.088$ and $\sigma_{int} = 0.614 \pm 0.066$, corresponding to $L_0 \propto t_b^{-0.944 \pm 0.098} E_{\gamma,iso}^{0.369 \pm 0.088}$. The fitting results of the parameters are shown in Table 1.

3.2. Calibrating $L_0 - t_b - E_{\gamma,iso}$ correlation

In above section, due to the lack of GRB data at low-redshift, we have fixed the values of Ω_m and H_0 to calculate the luminosity distance. Therefore, one have to deal with the "circularity problem" when using the correlations of GRBs to constrain cosmological parameters. Many methods have been developed to calibrate the correlation of GRBs in order to tackle this issue (Capozziello & Izzo 2008; Kodama et al. 2008; Liang et al. 2008; Wang & Dai 2011; Wang et al. 2016; Amati et al. 2019). Here we will use the gaussian process

¹ In fact, a is a constant. b and c are actually the power-law indices of t_b and $E_{\gamma,iso}$ when we consider L_0 as a power law functions of t_b and $E_{\gamma,iso}$

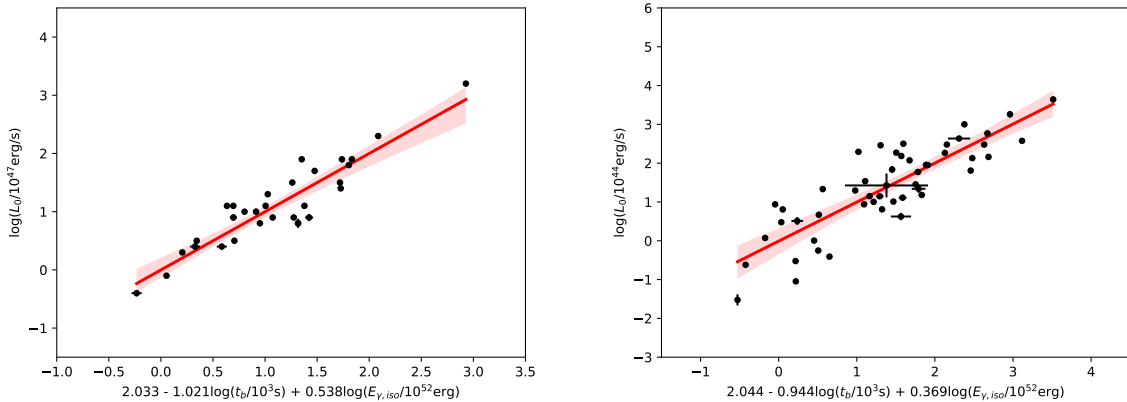


Figure 1. The correlation between luminosity L_0 , the end time t_b and the isotropic energy release $E_{\gamma,iso}$ ($L_0 - t_b - E_{\gamma,iso}$). Here we have set $\Omega_m = 0.3$ and $H_0 = 70 \text{ km s}^{-1} \text{ Mpc}^{-1}$ for calculating the luminosity from the measured flux. The data points are the GRBs in X-ray (left) and optical samples (right). The red line corresponds to the best fitting values of the data points with a 95% confidence band.

Table 1. The best fitting results of the parameters for different correlations

$L_0 - t_b - E_{\gamma,iso}$ correlation	a	b	c	σ_{int}
X-ray sample	2.033 ± 0.144	-1.021 ± 0.092	0.538 ± 0.144	0.303 ± 0.043
Optical sample	2.044 ± 0.149	-0.944 ± 0.098	0.369 ± 0.088	0.614 ± 0.066
Calibrated $L_0 - t_b - E_{\gamma,iso}$ correlation	a	b	c	σ_{int}
X-ray sample	1.948 ± 0.203	-1.047 ± 0.122	0.426 ± 0.174	0.317 ± 0.078
Optical sample	1.958 ± 0.153	-1.027 ± 0.106	0.423 ± 0.088	0.558 ± 0.070
$L_0 - t_b - E_{p,i}$ correlation	a'	b'	c'	σ_{int}
X-ray sample	1.556 ± 0.487	-0.963 ± 0.117	0.266 ± 0.163	0.363 ± 0.054
Optical sample	0.860 ± 0.445	-0.900 ± 0.104	0.604 ± 0.172	0.637 ± 0.070
Calibrated $L_0 - t_b - E_{p,i}$ correlation	a'	b'	c'	σ_{int}
X-ray sample	1.833 ± 0.852	-1.008 ± 0.154	0.126 ± 0.333	0.404 ± 0.095
Optical sample	0.741 ± 0.480	-1.012 ± 0.121	0.649 ± 0.190	0.616 ± 0.080

(GP) method to calibrate the Dainotti Relation (Hu et al. 2021; Wang et al. 2022). This method is based on the fact that objects with the same redshift have the same luminosity distance in any model of the Universe. In this work, GP regression is implemented using the public code GaPP (Seikel et al. 2012). The calibrated correlation obtained in this method is model-independent. The process of calibrating correlation is divided into two main steps. First, $H(z)$ data (Yu et al. 2018) are used to calibrate the luminosity distance d_L of GRBs with low redshift. According to the equations (2) and (6), the newly calculated $E_{\gamma,iso}$ and L_0 are obtained, and then the best fitting values of the $L_0 - t_b - E_{\gamma,iso}$ correlation parameters for the calibrated low redshift GRBs are obtained. Second, the model-independent distance modulus of higher redshifts are calculated using the cal-

ibrated parameters of fitting results of $L_0 - t_b - E_{\gamma,iso}$ correlation in the lower redshifts.

We perform the GP process to reconstruct the continuous function $H(z)$, and one can refer to, e.g., Seikel et al. (2012) and Wang et al. (2022) for more detailed discussions. Using the GP method, one can get the luminosity distance with respect to the Hubble parameter $H(z)$,

$$d_L(z) = c(1+z) \int_0^z \frac{dz}{H(z)}. \quad (10)$$

After obtaining the continuous function, the values of $H(z)$ at different redshifts can be calculated. Fig. 2 shows the reconstruction results of the $H(z)$ curve. According to the equation (10), we can get the corresponding redshift luminosity distance of each GRB, and then we get the L_0 and $E_{\gamma,iso}$ from the equations (2) and (6), which can be used to fit the parameters a , b and

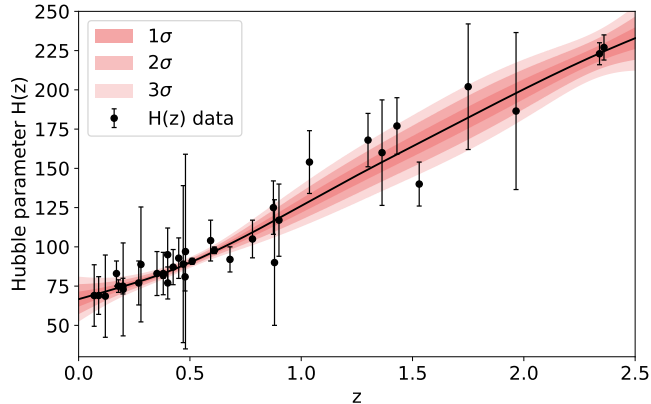


Figure 2. Reconstruction results of $H(z)$. The black line is the smoothed $H(z)$ function with GP method. The shaded regions correspond to 1σ , 2σ and 3σ errors. The data points are 36 $H(z)$ data in the redshift range of $0.07 \leq z \leq 2.36$. (Source: Figure 4 in Hu et al. (2021).)

c of the correlation $L_0 - t_b - E_{\gamma,iso}$. We have used 36 $H(z)$ data collected by Yu et al. (2018) in the redshift range of $0.17 < z < 2.36$ for the calibration process. Therefore, we can estimate the luminosity distance of GRBs in the redshift of $z \lesssim 2.50$. There are 14 GRBs of X-ray sample and 38 GRBs of optical sample in this redshift range, and then we use the two selected samples to obtain the model-independent luminosity distances, which can be used to calibrate the $L_0 - t_b - E_{\gamma,iso}$ correlation for the X-ray and optical samples, respectively. The corresponding results after calibration are shown in Figure 3. The best fitting results of the selected X-ray sample are $a = 1.948 \pm 0.203$, $b = -1.047 \pm 0.122$, $c = 0.426 \pm 0.174$ and $\sigma_{\text{int}} = 0.317 \pm 0.078$, corresponding to $L_0 \propto t_b^{-1.047 \pm 0.122} E_{\gamma,iso}^{0.426 \pm 0.174}$. For the selected optical sample, the best fitting results are $a = 1.958 \pm 0.153$, $b = -1.027 \pm 0.106$, $c = 0.423 \pm 0.088$ and $\sigma_{\text{int}} = 0.558 \pm 0.070$, corresponding to $L_0 \propto t_b^{-1.027 \pm 0.106} E_{\gamma,iso}^{0.423 \pm 0.088}$. The fitting results of the parameters are shown in Table 1.

The $L_0 - t_b - E_{\gamma,iso}$ correlation calibrated in this way are model-independent and can be used to constrain cosmological parameters. For the optical sample, the correlation after calibration is tighter than that obtained by fitting the entire samples. Furthermore, for X-ray sample, the value of σ_{int} after calibration is slightly larger than that obtained for all samples. The reason could be that there are not enough data points for X-ray samples in lower redshifts, leading to the increasing of the internal dispersion.

In the process of constraining cosmological parameters by employing the calibrated correlation $L_0 - t_b - E_{\gamma,iso}$, we found that it is difficult to get robust constraints on cosmological parameters. The reasons of why $L_0 -$

$t_b - E_{\gamma,iso}$ correlation is not good cosmological probe has been discussed in Xu et al. (2021), and our results support that states. First, the method of extrapolating the calibration results from lower redshifts to higher redshifts may not be appropriate, due to the possible evolution of the $L_0 - t_b - E_{\gamma,iso}$ correlation. Second, the selected GRB samples that may have the same physical mechanism are not enough to be calibrated for lower redshifts, leading to the increase of the internal dispersion. Third, the calculations of both L_0 and $E_{\gamma,iso}$ depend on the luminosity distance d_L , which relies on the cosmological parameters. This means that cosmological effect may be largely cancelled out in the relationship, or the correlation is insensitive to the cosmological parameters.

3.3. Calibrating $L_0 - t_b - E_{p,i}$ correlation

We now investigate whether the $L_0 - t_b - E_{p,i}$ correlation can be used to probe the cosmological parameters, where $E_{p,i} = E_{p,obs} \times (1+z)$ is the spectral peak energy with the observed peak energy $E_{p,obs}$. For this correlation, we have collected data from the following literature : Si et al. (2018), Minaev & Pozanenko (2020), Xu et al. (2021) and Lan et al. (2021), and we have removed GRB190114A due to the lack of $E_{p,i}$ data.

We studied the $L_0 - t_b - E_{p,i}$ correlation using the same approach described in the previous section. The relation can be written as

$$\log \frac{L_0}{10^{47} \text{erg s}^{-1}} = a' + b' \log \frac{t_b}{10^3 \text{s}} + c' \log \frac{E_{p,i}}{\text{keV}}. \quad (11)$$

For the X-ray sample, the best fitting results are $a' = 1.556 \pm 0.487$, $b' = -0.963 \pm 0.117$, $c' = 0.266 \pm 0.163$ and $\sigma_{\text{int}} = 0.363 \pm 0.054$, corresponding to $L_0 \propto t_b^{-0.977 \pm 0.111} E_{p,i}^{0.240 \pm 0.141}$. For the optical sample, the

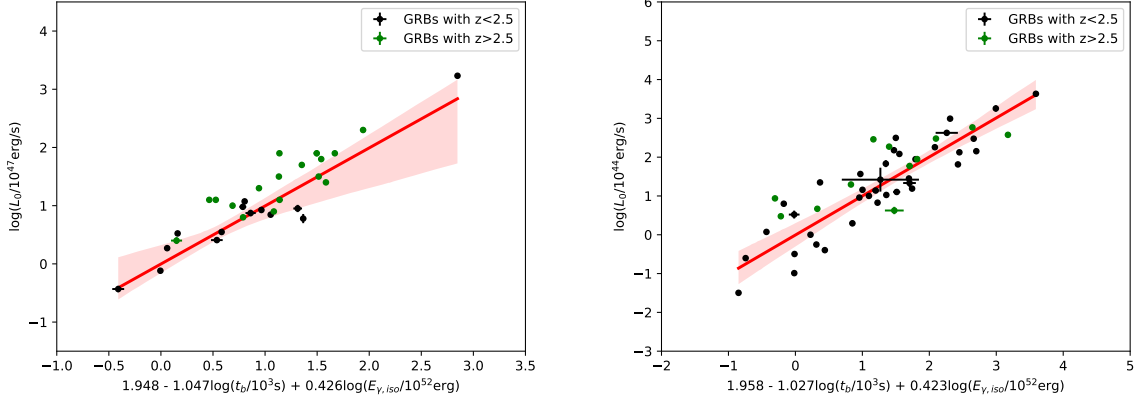


Figure 3. The calibrated $L_0 - t_b - E_{\gamma,iso}$ correlation for 14 X-ray sample (left) and 38 optical sample (right). GRBs with $z > 2.5$ are also shown (green dots). The red line is the best fitting line for data points, with a 95% confidence band.

best fitting result are $a' = 0.860 \pm 0.445$, $b' = -0.900 \pm 0.104$, $c' = 0.604 \pm 0.172$ and $\sigma_{\text{int}} = 0.637 \pm 0.070$, corresponding to $L_0 \propto t_b^{-0.900 \pm 0.104} E_{p,i}^{0.604 \pm 0.172}$. The corresponding fitting results are shown in Figure 4. It can be seen that there is a clear correlation between these three parameters. The fitting results of the parameters are shown in Table 1.

We also calibrated the three-parameter correlation using the selected data in the redshift range of $z < 2.5$ for the two sets of samples. The corresponding results after calibration are shown in Figure 5. For the X-ray sample, the best fitting result are $a' = 1.833 \pm 0.852$, $b' = -1.008 \pm 0.154$, $c' = 0.126 \pm 0.333$ and $\sigma_{\text{int}} = 0.404 \pm 0.095$, corresponding to $L_0 \propto t_b^{-1.008 \pm 0.154} E_{p,i}^{0.126 \pm 0.333}$. The best fitting result for the low redshift optical sample are $a' = 0.741 \pm 0.480$, $b' = -1.012 \pm 0.121$, $c' = 0.649 \pm 0.190$ and $\sigma_{\text{int}} = 0.616 \pm 0.080$, corresponding to $L_0 \propto t_b^{-1.012 \pm 0.121} E_{p,i}^{0.649 \pm 0.190}$. The corresponding corner diagrams can be found in Figure 6, and the fitting results of the parameters are shown in Table 1. We will use the calibrated $L_0 - t_b - E_{p,i}$ correlation for cosmological constraints.

4. CONSTRAINTS ON THE COSMOLOGICAL PARAMETERS USING THE THREE-PARAMETER CORRELATION

In the flat Λ CDM model, the distance modulus can be written as

$$\mu_{\text{th}} = 5 \log \frac{d_L}{\text{Mpc}} + 25 = 5 \log \frac{d_L}{\text{cm}} + 97.45. \quad (12)$$

From the equations (2) and (11) one can get the corresponding function to replace d_L in the equation (12). When optical sample is considered, the typical value of

L_0 is $10^{44} \text{erg s}^{-1}$. The corresponding observed distance can be defined as

$$\mu_{\text{obs}} = \frac{5}{2} \left[a + b(\log t_b - 3) + c \log E_{p,i} - \log \frac{4\pi F}{(1+z)} + 44 \right] - 97.45. \quad (13)$$

The uncertainty of μ_{obs} can be expressed as

$$\sigma_{\text{obs}} = \frac{5}{2} \left[\sigma_{\text{int}}^2 + \sigma_a^2 + \sigma_b^2 (\log t_b - 3)^2 + b^2 \left(\frac{\sigma_{t_b}}{t_b \ln 10} \right)^2 + c^2 \left(\frac{\sigma_{E_{p,i}}}{E_{p,i} \ln 10} \right)^2 + \left(\frac{\sigma_F}{F \ln 10} \right)^2 + \sigma_c^2 \log^2 E_{p,i} \right]^{1/2}, \quad (14)$$

where σ_i represents the error of different parameters derived as $\sqrt{(\sigma_u^2 + \sigma_d^2)/2}$, where σ_u and σ_d represent the upper and lower error of the parameters, respectively. The best-fitting parameters can be obtained by minimizing the χ^2 ,

$$\chi^2 = \sum_{j=1}^N \frac{[\mu_{\text{obs}}(z) - \mu_{\text{th}}(\Omega_i, z)]^2}{\sigma_{\text{obs}}^2}, \quad (15)$$

where N is the number of samples in each category. μ_{obs} and σ_{obs} can be calculated from the equations (13) and (14), respectively. $\mu_{\text{th}}(\Omega_i, z)$ is the theoretical distance modulus, and Ω_i represent the cosmological parameters needed to be constrained.

In general, the luminosity distance can be written as

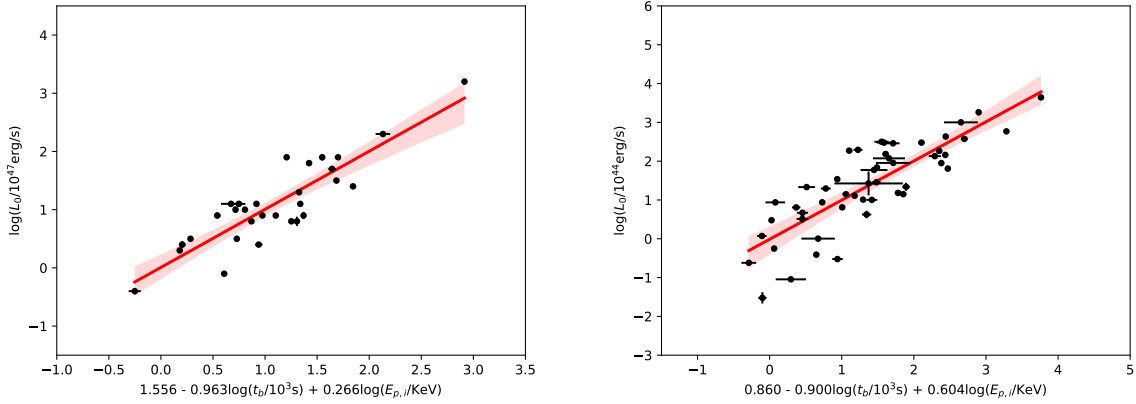


Figure 4. The correlation between luminosity L_0 , the end time t_b and the spectral peak energy $E_{p,i}$ ($L_0 - t_b - E_{p,i}$). The data points are the GRBs in X-ray (left) and optical samples (right). The red line corresponds to the best fitting values of the data points, with a 95% confidence band.

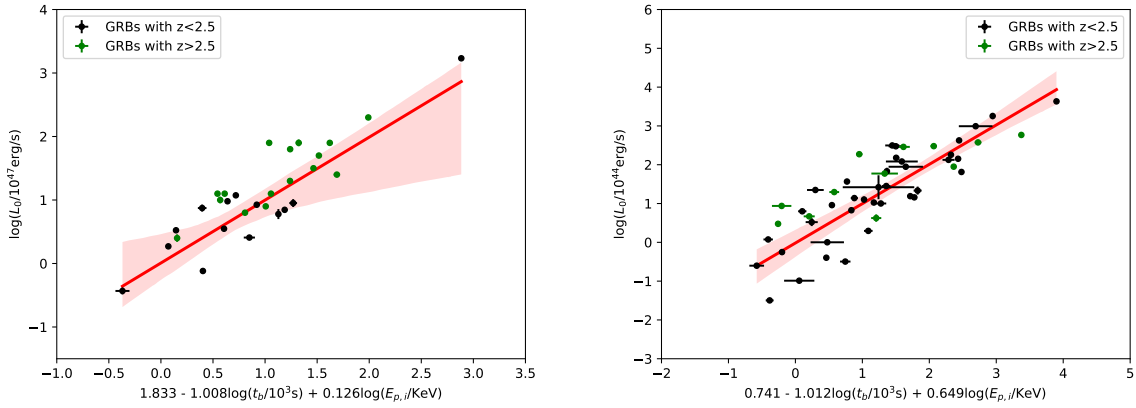


Figure 5. The calibrated $L_0 - t_b - E_{p,i}$ correlation for 14 X-ray sample (left) and 38 optical sample (right). GRBs with $z > 2.5$ are also plotted (green dots). The red line corresponds to the best fitting values of the data points, with a 95% confidence band.

$$d_L = \begin{cases} \frac{c(1+z)}{H_0} (-\Omega_k)^{-\frac{1}{2}} \sin \left[(-\Omega_k)^{-\frac{1}{2}} \int_0^z \frac{dz}{E(z)} \right] & \Omega_k < 0, \\ \frac{c(1+z)}{H_0} \int_0^z \frac{dz}{E(z)} & \Omega_k = 0, \\ \frac{c(1+z)}{H_0} \Omega_k^{-\frac{1}{2}} \sinh \left[\Omega_k^{-\frac{1}{2}} \int_0^z \frac{dz}{E(z)} \right] & \Omega_k > 0, \end{cases} \quad (16)$$

where Ω_k stands for the curvature of space. $E(z)$ can be expressed as

$$E(z) = \sqrt{\Omega_m(1+z)^3 + (1 - \Omega_m - \Omega_\Lambda)(1+z)^2 + \Omega_\Lambda}. \quad (17)$$

Now one can get the corresponding theoretical distance modulus μ_{th} by taking the equation (16) into (12). Using the minimized equation (15), one can obtain the

constraints on the related parameters of the Λ CDM cosmological model.

Only employing the optical sample distributed in the redshift range of $0.13 \lesssim z \lesssim 4.67$, we get the best-fitting results of the cosmological parameter $\Omega_m = 0.697^{+0.402}_{-0.278}(1\sigma)$ for a flat universe model, as shown in the left panel of Fig. 7. For the non-flat model, the best-fitting results are $\Omega_m = 0.713^{+0.346}_{-0.278}$, $\Omega_\Lambda = 0.981^{+0.379}_{-0.580}(1\sigma)$, as shown in the right panel of Figure 7. We only combine the optical and X-ray samples to constrain the parameters. For a flat Λ CDM model, the left panel of Fig. 8 shows the best-fit matter density parameter $\Omega_m = 0.313^{+0.179}_{-0.125}(1\sigma)$. The best-fitting results $\Omega_m = 0.344^{+0.176}_{-0.112}$, $\Omega_\Lambda = 0.770^{+0.366}_{-0.416}(1\sigma)$ for a non-flat Λ CDM model are shown in the right of Figure 8. The final constraints on the cosmological parameters can be

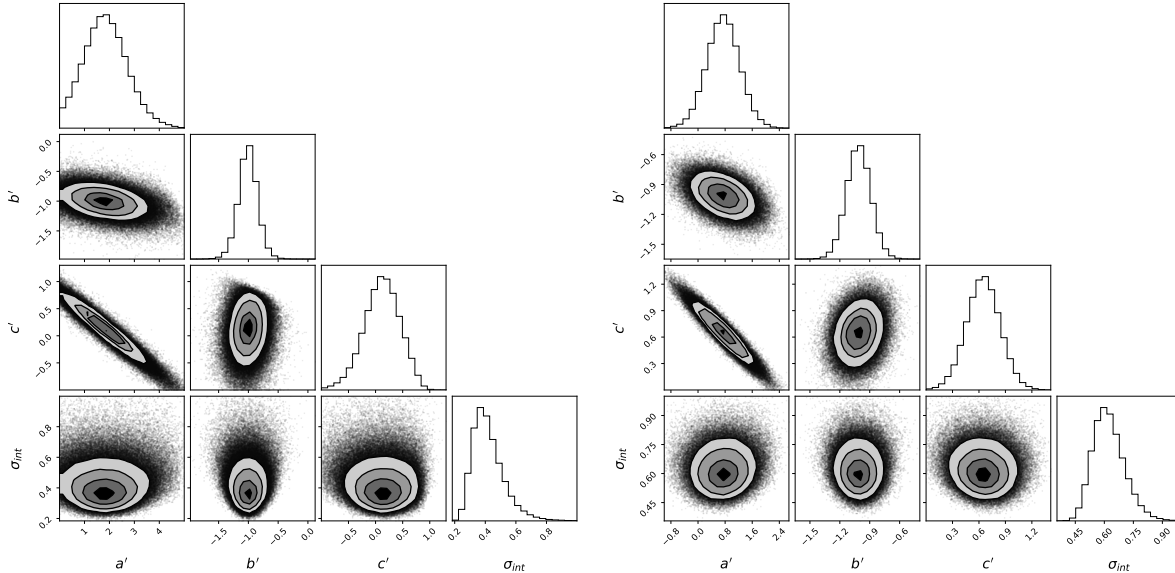


Figure 6. The corner diagrams of the related parameters used in Fig. 5 for the calibrated $L_0 - t_b - E_{p,i}$ correlation for the X-ray sample (left) and optical sample (right). The shaded regions correspond to 1σ , 2σ and 3σ errors.

found in Table 2. It is worth noting that the combined samples reduce the uncertainties of the parameters compared to the optical GRB sample alone. Note that the constraints on the cosmological parameters obtained from the X-ray and optical samples of GRBs are weaker than that obtained from SNe Ia and X-ray sample only of Wang et al. (2022). There are several reasons for this. One is that the optical sample size is not large enough. The second is that the optical sample might be not clean. Compared with X-ray, optical band has lower radiation efficiency and more complex radiation composition. In the future, with more powerful telescopes to obtain multi-band spectra, we should be able to reveal the intrinsic mechanism. It is also hoped that the optical samples can be classified more carefully by the spectral index and light-curve shapes. The third point is based on the fact that there are measurement inaccuracies in the three parameters of L_0 , t_b , and $E_{p,i}$ (Si et al. 2018; Liang et al. 2010; Li et al. 2012; Zhao et al. 2020).

Additionally, the Hubble diagram derived from the $L_0 - t_b - E_{\gamma,iso}$ correlation for all the calibrated samples is shown in the left panel of Figure 9. It can be seen from the diagram that the points at high-redshift of all the samples are highly dispersive and accompanied by large error bars, making it difficult to obtain meaningful constraints on the cosmological parameters with this correlation. In the right of Figure 9, we present the calibrated GRB Hubble diagram from the $L_0 - t_b - E_{p,i}$ correlation. It can be seen that the dispersion of the data points in the Hubble diagram from the $L_0 - t_b - E_{p,i}$ correlation

is smaller than that in the $L_0 - t_b - E_{\gamma,iso}$ correlation. It should be also noted that the error bar of the data points is large. Anyway, although the $L_0 - t_b - E_{p,i}$ correlation alone can not be used to constrain the cosmological parameters accurately, it can be used as a new way and a useful supplement to the current widely used cosmological probes.

5. CONCLUSIONS

We have investigated whether the three-parameter correlation in GRBs, $L_0 - t_b - E_{\gamma,iso}(E_{p,i})$, can be used to constrain the cosmological parameters. We found that $L_0 - t_b - E_{p,i}$ correlation is better than $L_0 - t_b - E_{\gamma,iso}$ for limiting the cosmological parameters. We have selected two groups of GRB samples: one group is composed of 31 long GRBs with X-ray plateau followed by a normal decay phase with a decay index of about -2. The other group is comprised of 50 optical samples with light curves from a shallow decay (or a slight rising phase) to normal decay (or an even steeper decay). The GRBs selected by classification of decay phase are generally assumed to have the same physical origin. We have used the GP method to calibrate the three-parameter correlation, and then the cosmological parameters are constrained by using the selected samples. Employing the optical sample, we get the best-fitting result of the parameter $\Omega_m = 0.697_{-0.278}^{+0.402}(1\sigma)$ for a flat universe model. For the non-flat model, the best-fitting results are $\Omega_m = 0.713_{-0.278}^{+0.346}$, $\Omega_\Lambda = 0.981_{-0.580}^{+0.379}(1\sigma)$. Utilizing all the optical and X-ray sample, for a flat Λ CDM model, the best-fitting matter density param-

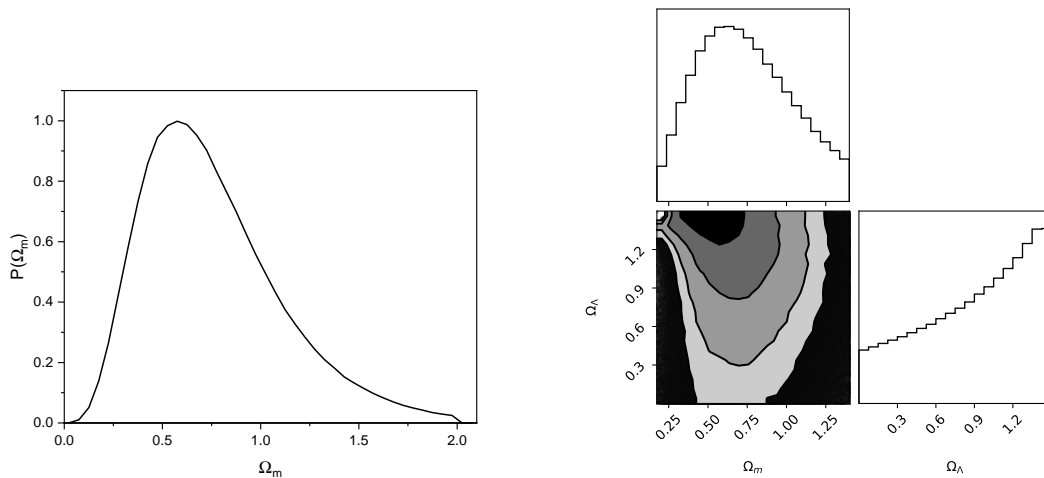


Figure 7. Constraints on the cosmological parameters in Λ CDM universe model using the optical sample. The left panel shows the probability distribution of Ω_m in the flat Λ CDM model. The right panel shows the constraints on Ω_m and Ω_Λ in the non-flat Λ CDM model.

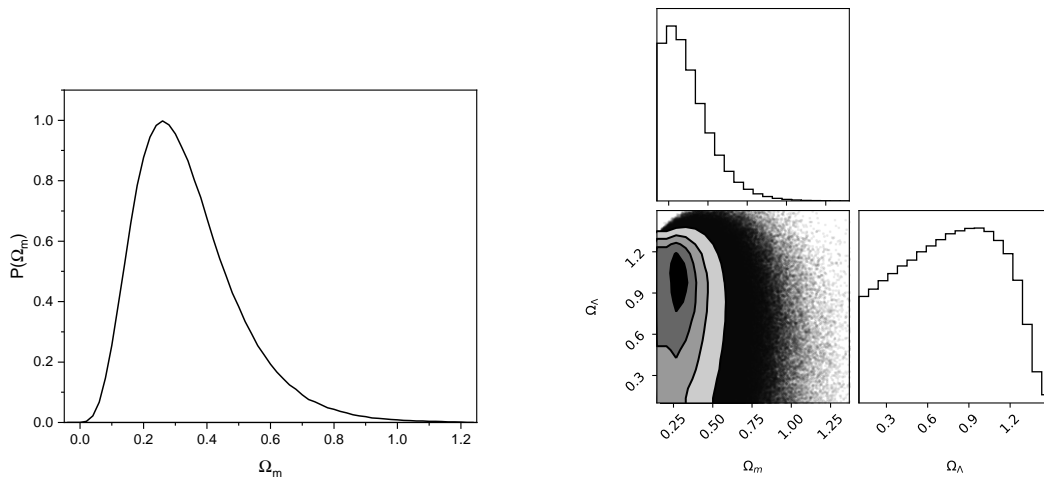


Figure 8. Constraints on the cosmological parameters in Λ CDM model using the optical and X-ray samples. The left panel shows the probability distribution of Ω_m in the flat Λ CDM model. The right panel shows the constraints on Ω_m and Ω_Λ in the non-flat Λ CDM model.

eter is $\Omega_m = 0.313^{+0.179}_{-0.125}(1\sigma)$, and $\Omega_m = 0.344^{+0.176}_{-0.112}$, $\Omega_\Lambda = 0.770^{+0.366}_{-0.416}(1\sigma)$ for a non-flat Λ CDM model.

Based on the results, we found that the constraints on the cosmological parameters obtained from GRBs of X-ray and optical samples are weaker than those obtained from SNe Ia. Therefore, $L_0 - t_b - E_{p,i}$ correlation can not simply be used to accurately measure the cosmological parameters at present, but can be seen as a supplement of cosmological probes. We also found that the final constraints from the X-ray sample are not as tight as that of the combined sample, and there is a relatively

large dispersion for the $L_0 - t_b - E_{p,i}$ correlation. Our results support that selecting GRB samples from possible identical physical mechanism is crucial for cosmological purposes.

In the future, it is expected that more sophisticated multiband detectors can detect much more high-redshift GRBs, which will help us better study GRBs and the high-redshift universe. In addition, the corresponding parameters, e.g., L_0 , t_b and $E_{p,i}$, can be better determined, and then the $L_0 - t_b - E_{p,i}$ correlation could be used to constrain the cosmological parameters better.

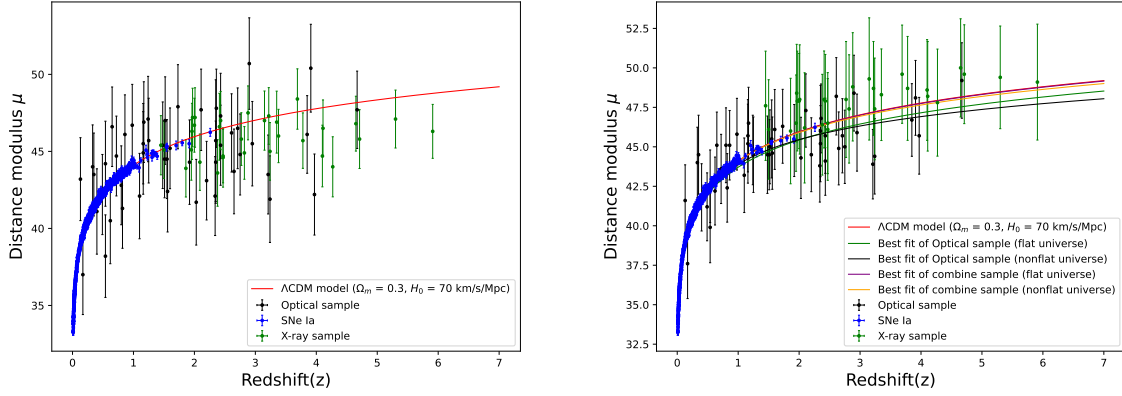


Figure 9. Calibrated GRB Hubble diagram using the $L_0 - t_b - E_{\gamma,iso}$ correlation (left) and $L_0 - t_b - E_{p,i}$ correlation (right). The black and green points represent optical and X-ray samples, respectively. Blue points are SNe Ia from the Pantheon sample. The solid red line corresponds to the theoretical distance modulus calculated for a flat Λ CDM model with $H_0 = 70 \text{ km s}^{-1} \text{ Mpc}^{-1}$ and $\Omega_m = 0.3$. For a flat universe, the best fit from the optical sample is shown as a green line and the best fit from the combine sample is shown as a purple line. For the nonflat universe, the black line shows the best fit from the optical sample, and the orange line shows the best fit from the combine sample.

Table 2. Constraints on the cosmological parameters for different universe model and GRB samples

Flat Λ CDM model	Ω_m	
Optical sample	$0.697^{+0.402}_{-0.278}$	
X-ray + Optical sample	$0.313^{+0.179}_{-0.125}$	
Non-flat Λ CDM model	Ω_m	Ω_Λ
Optical sample	$0.713^{+0.346}_{-0.278}$	$0.981^{+0.379}_{-0.580}$
X-ray + Optical sample	$0.344^{+0.176}_{-0.112}$	$0.770^{+0.366}_{-0.416}$

6. ACKNOWLEDGMENTS

We thank the referee for helpful comments. This work is supported by the National Natural Science Foundation of China (Grant Nos. U2038106,

12273009), Shandong Provincial Natural Science Foundation (ZR2021MA021), Jiangsu Program for Excellent Postdoctoral Talent (20220ZB59) and China Postdoctoral Science Foundation (2022M721561).

REFERENCES

- Abbott, B. P., Abbott, R., Abbott, T. D., et al. 2017, ApJL, 848, L13. doi:10.3847/2041-8213/aa920c
- Amati, L., Frontera, F., Tavani, M., et al. 2002, A&A, 390, 81. doi:10.1051/0004-6361:20020722
- Amati, L., D’Agostino, R., Luongo, O., et al. 2019, MNRAS, 486, L46. doi:10.1093/mnrasl/slz056
- Amati, L. & Della Valle, M. 2013, International Journal of Modern Physics D, 22, 1330028. doi:10.1142/S0218271813300280
- Band, D., Matteson, J., Ford, L., et al. 1993, ApJ, 413, 281. doi:10.1086/172995
- Cao, S., Dainotti, M., & Ratra, B. 2022a, MNRAS, 516, 1386. doi:10.1093/mnras/stac2170
- Cao, S., Dainotti, M., & Ratra, B. 2022b, MNRAS, 512, 439. doi:10.1093/mnras/stac517
- Cao, S., Khadka, N., & Ratra, B. 2022c, MNRAS, 510, 2928. doi:10.1093/mnras/stab3559
- Capozziello, S. & Izzo, L. 2008, A&A, 490, 31. doi:10.1051/0004-6361:200810337
- Cardone, V. F., Capozziello, S., & Dainotti, M. G. 2009, MNRAS, 400, 775. doi:10.1111/j.1365-2966.2009.15456.x
- Cardone, V. F., Dainotti, M. G., Capozziello, S., et al. 2010, MNRAS, 408, 1181. doi:10.1111/j.1365-2966.2010.17197.x
- Carroll, S. M. 2001, Living Reviews in Relativity, 4, 1. doi:10.12942/lrr-2001-1
- Cucchiara, A., Levan, A. J., Fox, D. B., et al. 2011, ApJ, 736, 7. doi:10.1088/0004-637X/736/1/7

- D'Agostini, G. 2005, physics/0511182.
doi:10.48550/arXiv.physics/0511182
- Dai, Z. G., Liang, E. W., & Xu, D. 2004, ApJL, 612, L101.
doi:10.1086/424694
- Dai, Z. G. & Lu, T. 1998a, PhRvL, 81, 4301.
doi:10.1103/PhysRevLett.81.4301
- Dai, Z. G. & Lu, T. 1998b, A&A, 333, L87.
doi:10.48550/arXiv.astro-ph/9810402
- Dainotti, M. G., Cardone, V. F., & Capozziello, S. 2008, MNRAS, 391, L79. doi:10.1111/j.1745-3933.2008.00560.x
- Dainotti, M. G., Ostrowski, M., & Willingale, R. 2011, MNRAS, 418, 2202. doi:10.1111/j.1365-2966.2011.19433.x
- Dainotti, M. G., Nielson, V., Sarracino, G., et al. 2022a, MNRAS, 514, 1828. doi:10.1093/mnras/stac1141
- Dainotti, M. G., Sarracino, G., & Capozziello, S. 2022b, PASJ, 74, 1095. doi:10.1093/pasj/psac057
- Dainotti, M. G., Cardone, V. F., Piedipalumbo, E., et al. 2013, MNRAS, 436, 82. doi:10.1093/mnras/stt1516
- Dainotti, M. G., Hernandez, X., Postnikov, S., et al. 2017, ApJ, 848, 88. doi:10.3847/1538-4357/aa8a6b
- Dainotti, M. G., Postnikov, S., Hernandez, X., et al. 2016, ApJL, 825, L20. doi:10.3847/2041-8205/825/2/L20
- Deng, C., Huang, Y.-F., & Xu, F. 2023, ApJ, 943, 126. doi:10.3847/1538-4357/acaefd
- Fan, Y.-Z. & Xu, D. 2006, MNRAS, 372, L19.
doi:10.1111/j.1745-3933.2006.00217.x
- Foreman-Mackey, D., Hogg, D. W., Lang, D., et al. 2013, PASP, 125, 306. doi:10.1086/670067
- Gehrels, N., Ramirez-Ruiz, E., & Fox, D. B. 2009, ARA&A, 47, 567. doi:10.1146/annurev.astro.46.060407.145147
- Gehrels, N., Chincarini, G., Giommi, P., et al. 2004, ApJ, 611, 1005. doi:10.1086/422091
- Ghirlanda, G., Ghisellini, G., Lazzati, D., et al. 2004a, ApJL, 613, L13. doi:10.1086/424915
- Ghirlanda, G., Ghisellini, G., & Lazzati, D. 2004b, ApJ, 616, 331. doi:10.1086/424913
- Ghisellini, G., Nardini, M., Ghirlanda, G., et al. 2009, MNRAS, 393, 253. doi:10.1111/j.1365-2966.2008.14214.x
- Hu, J. P., Wang, F. Y., & Dai, Z. G. 2021, MNRAS, 507, 730. doi:10.1093/mnras/stab2180
- Izzo, L., Muccino, M., Zaninoni, E., et al. 2015, A&A, 582, A115. doi:10.1051/0004-6361/201526461
- Jia, X. D., Hu, J. P., Yang, J., et al. 2022, MNRAS, 516, 2575. doi:10.1093/mnras/stac2356
- Khadka, N., Luongo, O., Muccino, M., et al. 2021, JCAP, 2021, 042. doi:10.1088/1475-7516/2021/09/042
- Klebesadel, R. W., Strong, I. B., & Olson, R. A. 1973, ApJL, 182, L85. doi:10.1086/181225
- Kodama, Y., Yonetoku, D., Murakami, T., et al. 2008, MNRAS, 391, L1. doi:10.1111/j.1745-3933.2008.00508.x
- Kouveliotou, C., Meegan, C. A., Fishman, G. J., et al. 1993, ApJL, 413, L101. doi:10.1086/186969
- Kumar, P. & Zhang, B. 2015, PhR, 561, 1.
doi:10.1016/j.physrep.2014.09.008
- Lamb, D. Q. & Reichart, D. E. 2000, ApJ, 536, 1.
doi:10.1086/308918
- Lan, G.-X., Wei, J.-J., Zeng, H.-D., et al. 2021, MNRAS, 508, 52. doi:10.1093/mnras/stab2508
- Levine, D., Dainotti, M., Zvonarek, K. J., et al. 2022, ApJ, 925, 15. doi:10.3847/1538-4357/ac4221
- Li, L., Liang, E.-W., Tang, Q.-W., et al. 2012, ApJ, 758, 27. doi:10.1088/0004-637X/758/1/27
- Li, Z., Zhang, B., & Liang, N. 2023a, MNRAS.
doi:10.1093/mnras/stad838
- Li, X.-J., Zhang, W.-L., Yi, S.-X., et al. 2023b, ApJS, 265, 56. doi:10.3847/1538-4365/acc398
- Liang, E.-W., Zhang, B.-B., & Zhang, B. 2007, ApJ, 670, 565. doi:10.1086/521870
- Liang, E.-W., Yi, S.-X., Zhang, J., et al. 2010, ApJ, 725, 2209. doi:10.1088/0004-637X/725/2/2209
- Liang, E. & Zhang, B. 2006, MNRAS, 369, L37.
doi:10.1111/j.1745-3933.2006.00169.x
- Liang, E. & Zhang, B. 2005, ApJ, 633, 611.
doi:10.1086/491594
- Liang, N., Xiao, W. K., Liu, Y., et al. 2008, ApJ, 685, 354.
doi:10.1086/590903
- Liang, N., Li, Z., Xie, X., et al. 2022, ApJ, 941, 84.
doi:10.3847/1538-4357/aca08a
- Liu, Y., Liang, N., Xie, X., et al. 2022, ApJ, 935, 7.
doi:10.3847/1538-4357/ac7de5
- Lü, H.-J. & Zhang, B. 2014, ApJ, 785, 74.
doi:10.1088/0004-637X/785/1/74
- MacFadyen, A. I., Woosley, S. E., & Heger, A. 2001, ApJ, 550, 410. doi:10.1086/319698
- MacFadyen, A. I. & Woosley, S. E. 1999, ApJ, 524, 262.
doi:10.1086/307790
- Metzger, B. D., Giannios, D., Thompson, T. A., et al. 2011, MNRAS, 413, 2031. doi:10.1111/j.1365-2966.2011.18280.x
- Minaev, P. Y. & Pozanenko, A. S. 2020, MNRAS, 492, 1919. doi:10.1093/mnras/stz3611
- Mészáros, P. 2006, Reports on Progress in Physics, 69, 2259. doi:10.1088/0034-4885/69/8/R01
- Nousek, J. A., Kouveliotou, C., Grupe, D., et al. 2006, ApJ, 642, 389. doi:10.1086/500724
- O'Brien, P. T., Willingale, R., Osborne, J., et al. 2006, ApJ, 647, 1213. doi:10.1086/505457
- Paczyński, B. 1998, ApJL, 494, L45. doi:10.1086/311148
- Peebles, P. J. E. 1984, ApJ, 284, 439. doi:10.1086/162425
- Perlmutter, S., Aldering, G., Goldhaber, G., et al. 1999, ApJ, 517, 565. doi:10.1086/307221

- Phillips, M. M. 1993, *ApJL*, 413, L105. doi:10.1086/186970
- Planck Collaboration, Aghanim, N., Akrami, Y., et al. 2020, *A&A*, 641, A6. doi:10.1051/0004-6361/201833910
- Planck Collaboration, Ade, P. A. R., Aghanim, N., et al. 2016, *A&A*, 594, A13. doi:10.1051/0004-6361/201525830
- Planck Collaboration, Ade, P. A. R., Aghanim, N., et al. 2014, *A&A*, 571, A16. doi:10.1051/0004-6361/201321591
- Postnikov, S., Dainotti, M. G., Hernandez, X., et al. 2014, *ApJ*, 783, 126. doi:10.1088/0004-637X/783/2/126
- Qin, Y., Liang, E.-W., Liang, Y.-F., et al. 2013, *ApJ*, 763, 15. doi:10.1088/0004-637X/763/1/15
- Riess, A. G., Filippenko, A. V., Challis, P., et al. 1998, *AJ*, 116, 1009. doi:10.1086/300499
- Rowlinson, A., O'Brien, P. T., Metzger, B. D., et al. 2013, *MNRAS*, 430, 1061. doi:10.1093/mnras/sts683
- Schaefer, B. E. 2007, *ApJ*, 660, 16. doi:10.1086/511742
- Scolnic, D. M., Jones, D. O., Rest, A., et al. 2018, *ApJ*, 859, 101. doi:10.3847/1538-4357/aab9bb
- Seikel, M., Clarkson, C., & Smith, M. 2012, *JCAP*, 2012, 036. doi:10.1088/1475-7516/2012/06/036
- Si, S.-K., Qi, Y.-Q., Xue, F.-X., et al. 2018, *ApJ*, 863, 50. doi:10.3847/1538-4357/aad08a
- Spergel, D. N., Verde, L., Peiris, H. V., et al. 2003, *ApJS*, 148, 175. doi:10.1086/377226
- Tang, C.-H., Huang, Y.-F., Geng, J.-J., et al. 2019, *ApJS*, 245, 1. doi:10.3847/1538-4365/ab4711
- Tang, Q.-W., Wang, K., Li, L., et al. 2021, *ApJ*, 922, 255. doi:10.3847/1538-4357/ac26ba
- Wang, F. Y. & Dai, Z. G. 2011, *A&A*, 536, A96. doi:10.1051/0004-6361/201117517
- Wang, F.-Y., Qi, S., & Dai, Z.-G. 2011, *MNRAS*, 415, 3423. doi:10.1111/j.1365-2966.2011.18961.x
- Wang, F. Y., Hu, J. P., Zhang, G. Q., et al. 2022, *ApJ*, 924, 97. doi:10.3847/1538-4357/ac3755
- Wang, F. Y., Dai, Z. G., & Liang, E. W. 2015, *NewAR*, 67, 1. doi:10.1016/j.newar.2015.03.001
- Wang, J. S., Wang, F. Y., Cheng, K. S., et al. 2016, *A&A*, 585, A68. doi:10.1051/0004-6361/201526485
- Wei, J.-J. & Wu, X.-F. 2017, *International Journal of Modern Physics D*, 26, 1730002. doi:10.1142/S0218271817300026
- Wei, J., Wu, X., Wang, F., et al. 2018, *Scientia Sinica Physica, Mechanica & Astronomica*, 48, 039505. doi:10.1360/SSPMA2017-00248
- Woosley, S. E. & Bloom, J. S. 2006, *ARA&A*, 44, 507. doi:10.1146/annurev.astro.43.072103.150558
- Woosley, S. E. 1993, *ApJ*, 405, 273. doi:10.1086/172359
- Xu, F., Tang, C.-H., Geng, J.-J., et al. 2021, *ApJ*, 920, 135. doi:10.3847/1538-4357/ac158a
- Xu, M. & Huang, Y. F. 2012, *A&A*, 538, A134. doi:10.1051/0004-6361/201117754
- Yi, S.-X., Wu, X.-F., Wang, F.-Y., et al. 2015, *ApJ*, 807, 92
- Yi, S.-X., Xi, S.-Q., Yu, H., et al. 2016, *ApJS*, 224, 20. doi:10.3847/0067-0049/224/2/20
- Yi, S.-X., Du, M., & Liu, T. 2022, *ApJ*, 924, 69. doi:10.3847/1538-4357/ac35e7
- Yonetoku, D., Murakami, T., Nakamura, T., et al. 2004, *ApJ*, 609, 935. doi:10.1086/421285
- Yu, H., Ratra, B., & Wang, F.-Y. 2018, *ApJ*, 856, 3. doi:10.3847/1538-4357/aab0a2
- Zhang, B. & Mészáros, P. 2001, *ApJL*, 552, L35. doi:10.1086/320255
- Zhang, B., Fan, Y. Z., Dyks, J., et al. 2006, *ApJ*, 642, 354. doi:10.1086/500723
- Zhao, W., Zhang, J.-C., Zhang, Q.-X., et al. 2020, *ApJ*, 900, 112. doi:10.3847/1538-4357/aba43a